Template-free synthesis of single-crystalline SmF_3 rattle-structured sub-micropumpkins

Zhiming Chen,[a] Zhirong Geng,[a] Zhiyang Zhang,[a] Zhihui Liu[b] and Zhilin Wang*[a]

Received 11th December 2009, Accepted 16th March 2010
DOI: 10.1039/b926254g

Single-crystalline SmF_3 sub-micropumpkins with a rattle-type structure have been successfully synthesized on a large scale by reaction of aqueous Sm^{3+} with ammonium fluoride in the presence of ethylenediaminetetraacetic acid (EDTA) at 110 °C for 16 h, which were confirmed by X-ray powder diffraction, energy dispersive X-ray analysis, transmission electron microscopy, and scanning electron microscopy. The reaction time and EDTA have been shown to play important roles in the formation of SmF_3 rattle-structured sub-microcrystals. A mechanism for the formation of the SmF_3 rattle-structured sub-micropumpkins *via* cooperation of an oriented aggregation process and Ostwald ripening has been proposed based on observations of time-dependent experiments. In addition, this crystal growth mode could be expanded to the synthesized Eu-doped SmF_3 rattle-structured sub-microcrystals. It is believed that the results of the present investigation may provide a versatile approach for designing and fabricating a wide range of nano/microcrystals.

Introduction

In the past few years, extensive research interest has been drawn to the design and fabrication of inorganic materials with specific morphologies and sizes because of their distinctive functional properties compared with bulk materials.[1–4] In particular, the recent synthesis of inorganic rattle-structured nano/micromaterials have aroused increasing attention due to their unique structure and interesting properties, thus having wide potential applications in lithium-ion batteries,[5–7] microreactors,[8,9] biomedical areas,[10,11] catalytic[12,13] and sensing devices.[14] The conventional method for the preparation of such structures is a template-assistant synthetic methodology, which involves multi-step procedures: (1) prefabrication of core-shell spheres with two different substances serving as both template and core supplier; (2) coating the core-shell spheres with a layer of the third substance to form an egg-like composite with a three-layered structure similar to "yolk, egg white, and egg shell"; (3) removing the "egg white" region from the three-layered structures to form a rattle-type structure.[15] Normally, this method suffers from disadvantages related to high cost, tedious synthetic procedures and being environmentally unfriendly, which may restrict it being used in large-scale applications. To circumvent these difficulties, two template-free technologies, involving Ostwald ripening and Kirkendall effect, have been used to prepare rattle-structured metallic oxides,[5,14,16–18] hydroxides,[19] sulfides,[16,20–22] and transition-metal tetraoxometalates.[23–25] However, it still remains a major challenge to develop template-free, simple and one-step synthetic methods for rattle-structured nano/microstructures with designed chemical composition and controlled morphologies.

As an important category of functional materials, rare earth compounds have attracted much research interest due to their potential applications in optical telecommunication,[26–28] MALDI matrix,[29] catalysts,[30] bio-chemical probes and medical diagnostics[30–34] based on their unique properties arising from the transitions of 4f electrons. Among the various rare earth compounds, rare earth fluorides have many advantageous features which the conventional oxygen-based systems (*e.g.* oxides and inorganic salts) do not have, such as low vibrational energies, good optical transparency over a wide wavelength range, and are regarded as excellent host lattices for lanthanide ions.[35,36] Furthermore, it is widely documented that precise control of morphology, dimensionality, and size of the fluorides leads to enhanced luminescent properties of the crystals.[37,38] Therefore, different morphologies of rare-earth fluoride crystals based on different solution-based routes have been prepared, including fullerene-like lanthanide fluorides,[39,40] hexagonal and triangular YF_3 nanocrystals,[41] polyhedral YF_3 microcrystals,[36] monodispersed LaF_3 triangular nanoplates,[42] and EuF_3 nano/microcrystals with different morphologies.[29,43,44] However, to the best of our knowledge, there is no report available on rattle-structured rare earth fluorides.

Herein, we report a one-pot template-free hydrothermal route for the synthesis of pumpkin-like SmF_3 rattle-structured sub-microcrystals in large-scale by reaction of aqueous Sm^{3+} with ammonium fluoride in the presence of EDTA. It is found that EDTA in the reaction acted not only as a capped reagent but also as a speed-controller. A combined growth mechanism for these novel architectures has been discussed in detail. Moreover, this new type of rattle-structured crystal can be easily doped with Eu^{3+}, which may endow the sub-micropumpkin with novel properties.[45,46]

[a]*State Key Laboratory of Coordination Chemistry, School of Chemistry and Chemical Engineering, Nanjing University, Nanjing, 210093, People's Republic of China. E-mail: wangzl@nju.edu.cn; Fax: +86-25-83317761; Tel: +86-25-83686082*
[b]*School of Life Science, Nanjing University, Nanjing, 210093, People's Republic of China*

Results and discussion

The composition and phase purity of the products were examined by powder X-ray diffraction (XRD). Fig. 1a shows a typical XRD pattern of the sample obtained in the presence of EDTA at 110 °C for 16 h. The peaks can be readily assigned to hexagonal phase of SmF_3 by comparison with the JCPDS card file no. 72-1439. No other impurity peaks are detected in XRD pattern, indicating that the product is rather pure. Energy dispersive X-ray analysis (EDX) confirms that the sample is composed of only Sm and F, and atomic ratio for Sm : F is near 1 : 3, in agreement with the expected stoichiometry of the SmF_3 phase (Fig. 1b).

The morphology of the as-obtained product was investigated by field emission scanning electron microscopy (SEM) and transmission electron microscopy (TEM). Fig. 2a shows a typical SEM image of the product obtained at 110 °C for 16 h, and indicates that the sample is composed of uniform pumpkin-shaped structures with a diameter of 400 ± 100 nm and thick of 230 ± 70 nm. The enlargement shows that these pumpkin-shaped sub-microcrystals have a rattle-type structure (the inset in Fig. 2a). The rattle-structured nature of the sub-micropumpkins is further demonstrated by TEM image, as shown in Fig. 2b. It may be noted that most of the sub-micropumpkins are concentric core-shell configurations, while some are semi-hollow structures (highlighted by the circle). Of particular interest is to note that,

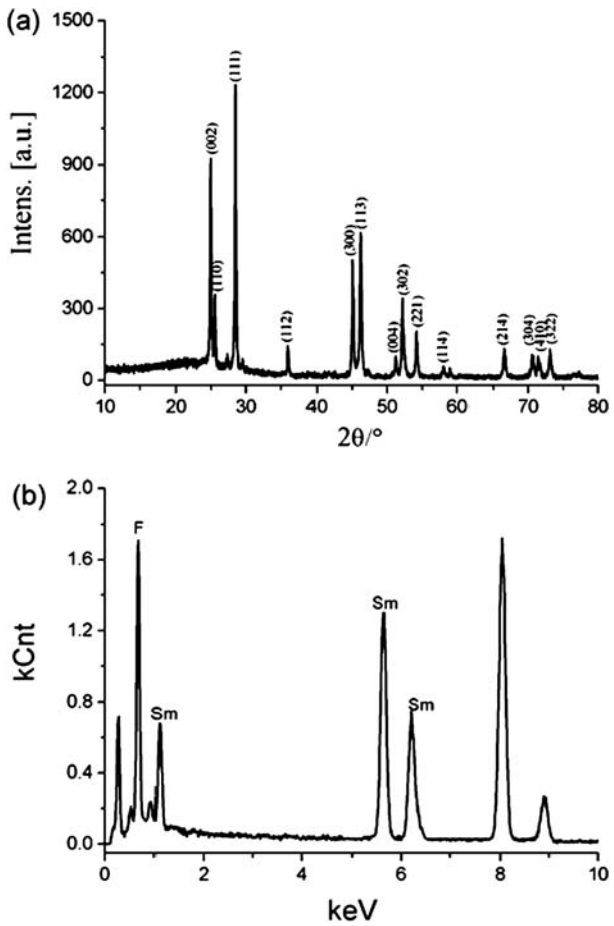

Fig. 1 (a) XRD pattern and (b) EDX analysis of the product obtained by reaction of Sm^{3+} with NH_4F in the presence of EDTA for 16 h.

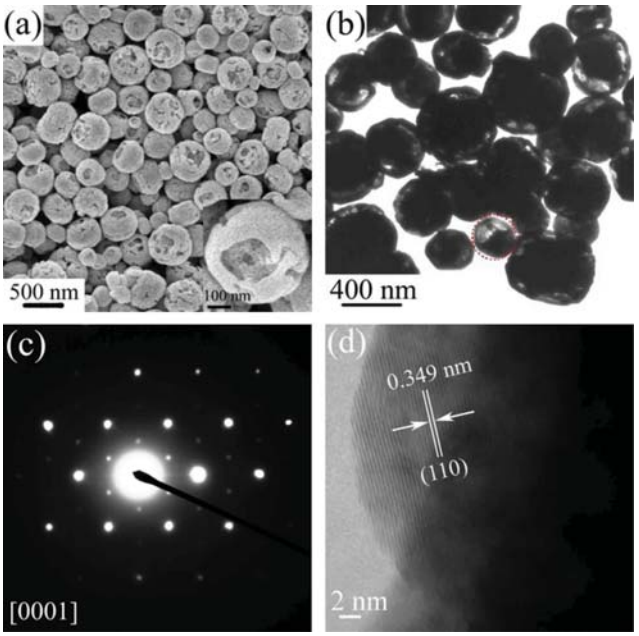

Fig. 2 (a) SEM and (b) TEM images of SmF_3 rattle-structured sub-micropumpkins prepared at 110 °C for 16 h; (c) SAED and (d) HRTEM images for an individual rattle-structured sub-micropumpkin. The red circle highlights the semi-hollow sub-micropumpkin.

when the whole particle was taken as the selected area for electron diffraction (SAED) measurement, the diffraction pattern exhibited a remarkable single-crystal feature as shown in Fig. 2c, in which the spots were indexed to $\{10\bar{1}0\}$ of hexagonal SmF_3. The high-resolution transmission electron microscopy (HRTEM) image of a single sub-microsphere (Fig. 2d), indicating that the distance between the adjacent lattice planes is 0.349 nm, is ascribed to (111) crystal planes of the hexagonal phase SmF_3.

In order to understand the formation process of the rattle-structured SmF_3 sub-micropumpkin, time-dependent experiments were carried out. Fig. 3 is a series of TEM and SEM images of the samples showing morphological evolution of the rattle-structured sub-micropumpkin. When the sample was prepared without heat treatment, only pristine particles are observed, as shown in Fig. 3a. The corresponding XRD pattern (Fig. 4d) indicates that the primary particles without hydrothermal treatment did not lead to any detectable crystalline phase. After 1 h hydrothermal treatment, the pristine particles aggregated together to form spherical aggregates (Fig. 3b). The XRD result (Fig. 4b) illustrates that the diffraction peaks of hexagonal phase of SmF_3 are found, indicating the formation of SmF_3 in these spherical aggregates. Through 2 h hydrothermal reaction, the pristine particles further congregated together. The SEM image illustrates that the surface of the aggregate is very coarse (Fig. 3c). The TEM image indicates that the pumpkin-like aggregates were solid (the inset in Fig. 3c). The corresponding XRD result confirms the formation of pure SmF_3 crystals, and the intensive diffraction peaks reveals the well crystallization of the products. With increasing reaction time to 6 h, the surface of sub-micropumpkins becomes less compact, and the outer crystallites become larger crystallites on attracting the smaller crystallites underneath (Fig. 3d). If the reaction time was

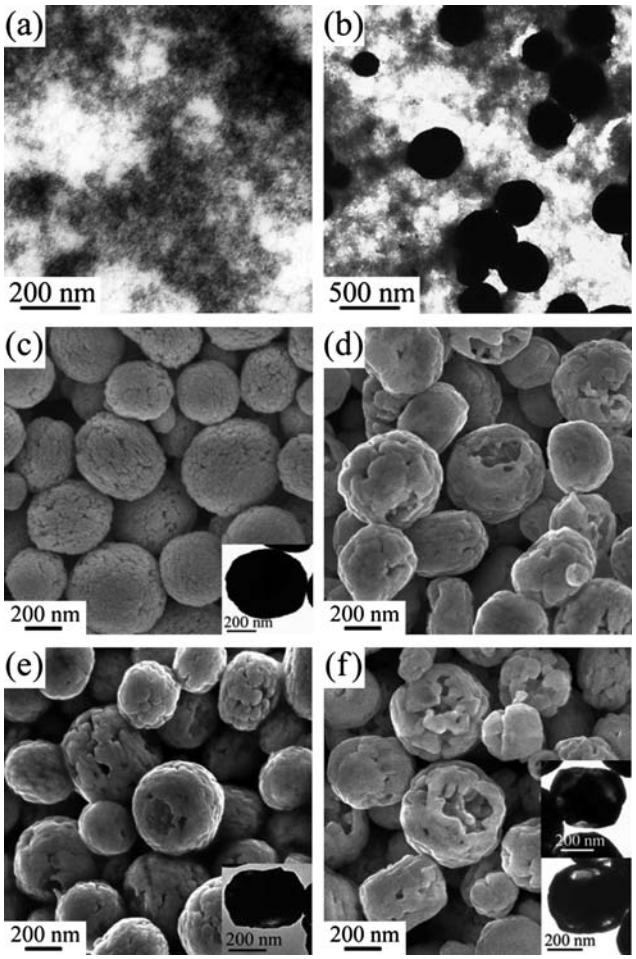

Fig. 3 TEM and SEM images of SmF_3 samples obtained by reaction of Sm^{3+} with NH_4F in the presence of EDTA (a) without hydrothermal treatment; (b–f) at 110 °C for 1, 2, 6, 8 and 12 h. Insets of (c), (e) and (f): TEM images of individual sub-micropumpkins.

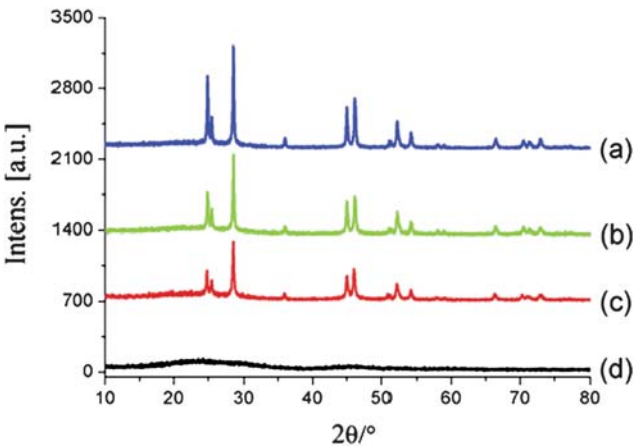

Fig. 4 XRD patterns for SmF_3 sub-micropumpkins prepared at 110 °C for (a) 12 h, (b) 2 h, (c) 1 h, and (d) without hydrothermal treatment.

prolonged to 8 h, SmF_3 sub-micropumpkins with a more coarse surface were obtained (Fig. 3e). Further prolonging the reaction time to 12 h resulted in distinct changes in particle morphology. In the typical SEM image of the products *via* 12 h of hydrothermal treatment, SmF_3 sub-micropumpkins with a rattle-type structure can be easily seen (Fig. 3f). Meanwhile, the intensities of the diffraction peaks of SmF_3 sub-micropumpkins increase significantly (Fig. 4a), indicating the enhancement of crystallization of the sub-micropumpkins. It is noticeable that during the formation process the size of these sub-micropumpkins does not change much.

Based on the above results, it is believed that a cooperation of an oriented aggregation process and Ostwald ripening should be the main driving force for the formation of these novel hierarchical architectures. It is well-known that the combined process of both oriented attachment and Ostwald ripening is an effective strategy for synthesis of single-crystalline hollow nano/micromaterials.[47,48] In our synthesis process, pumpkin-like aggregations with intrinsic size/density variations inside were formed *via* oriented attachment. Subsequently, the interior void space is gradually generated within the sub-micropumpkins *via* the symmetric/asymmetric ripening process. The formation process of the rattle-structured sub-micropumpkins is illustrated in Scheme 1. As depicted in Scheme 1a, SmF_3 pristine particles are produced and aggregated together to decrease the surface energy. Since the initially formed aggregates may act as the cores for the subsequent aggregation of the sub-micropumpkins, the center region of the solid sub-micropumpkins would be packed more densely than the outer. Then, the inner space can be created when the less stable parts (smaller or loosely packed crystallites) in the particles are undergoing mass transport through dissolving and recrystallizing. During the solid evacuation, crystallites located on the outermost surface would serve as starting points (or nucleation seeds) for the subsequent recrystallization process and continued crystal growth. As a consequence, the outer crystallites become larger on attracting the smaller crystallites from within, which results in a void space between the loosely packed exterior and the closely packed interior and thus the formation of rattle-type structures. Owing to the continued growth of the outer crystallites, the void space between the outer shell and the inner

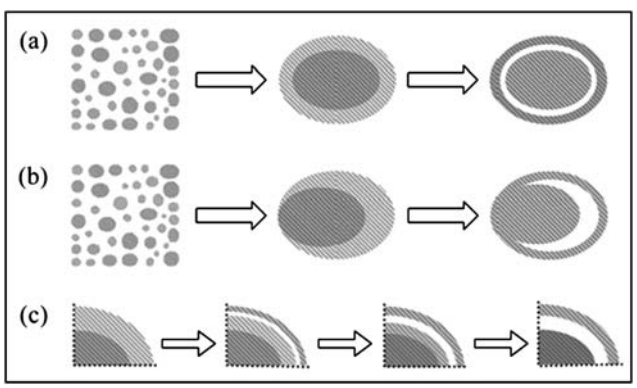

Scheme 1 (a) Formation of SmF_3 rattle-structured sub-micropumpkin *via* a cooperation of an oriented attachment and symmetric Ostwald ripening, (b) Formation of SmF_3 semi-hollow-structured sub-micropumpkin *via* a cooperation of an oriented attachment and asymmetric Ostwald ripening, (c) proposed model for the formation of the void space between core and shell *via* symmetric Ostwald ripening. Hashed lines: the cross-sectional plane of a sphere. Darker areas: larger and/or closely packed crystallites. Lighter areas: smaller and/or loosely packed crystallites. White areas: void space.

core will be enlarged and the core region will be trimmed down to smaller size because of the gradual mass diffusion when a longer reaction time is applied (Scheme 1c).

EDTA is an efficient chelator for rare earth ions. Its chelation constant ($\log\beta_1$) for Sm^{3+} is 17.14.[49] The presence of EDTA is found to be helpful for the formation of several types of nano/micromaterials, such as $NaLnF_4$ nanocrystals,[50] $NaYF_4$: Yb,Er nanocrystals,[31] and EuF_3 microcrystals.[29,44] To investigate the effect of EDTA on the morphology of SmF_3 particles in our synthetic method, the amount of EDTA was varied under the same precipitation condition to get a molar ratio of EDTA/Sm^{3+} of 0, 0.5, 1.0, and 2.5. As shown in Fig. 5a–d, it is visible that few spherical aggregate was formed in the starting solution with a low molar ratio of EDTA to Sm; while SmF_3 sub-micropumpkin with an unobvious rattle-type structure was obtained in the solution with a high molar ratio of EDTA to Sm. Furthermore, we also prepared a series of products under the same conditions *via* employing an equal amount of 1,6-hexanediamine and ammonium citrate as the additive instead of 1.71 mmol EDTA. It is found that SmF_3 rattle-structured sub-micropumpkin can be synthesized neither in the presence of 1,6-hexanediamine nor in the existence of ammonium citrate (Fig. 5e and 5f). Thus, we propose that EDTA plays two important roles in the formation of SmF_3 rattle-structured sub-micropumpkins: One is that EDTA may act as capped reagents and be adsorbed on the {0001} facets, further decreasing the surface energy of these facets, and consequently prohibiting the radial enlargement in the [0001] direction and driving the formation of pumpkin-like aggregates. The other is that chelation of Sm ions with EDTA should bring about decrease both in the nucleation process and in nuclei growth. In consequent, the decelerated crystallization may have helped the formation of the intrinsic density variations inside the solid pumpkin-like aggregates.

As is well known, Eu and Sm have very close ionic radii, and as a result, their physical and chemical properties are similar. So it can be speculated that SmF_3 rattle-structured sub-micropumpkins can be easily doped with large amounts of Eu^{3+}, which may endow these sub-micropumpkins with novel properties. To confirm this hypothesis, we prepared a series of products under the same conditions *via* employing the mixture of Sm_2O_3 and Eu_2O_3 with designated mole ratio as precursor instead of pure Sm_2O_3. The morphologies of the products were characterized by TEM (Fig. 6). It is observed that, with increasing the Eu doping concentration to 25–95%, the size of the products remains almost unchanged while the inner core trims down to smaller size, suggesting that Ostwald ripening is more efficient and core-hollowing also takes place much faster. Moreover, in the $Sm_{0.05}Eu_{0.95}F_3$ and $Sm_{0.25}Eu_{0.75}F_3$ samples, a few hollow hexagonal sub-micodiscs coexisting with rattle-structured sub-microdiscs were observed. This is because of the difference of the crystal growth habits arising from their solubility (Ksp) and chelation constant ($\log\beta_1$) for EDTA.[49] Previous investigation

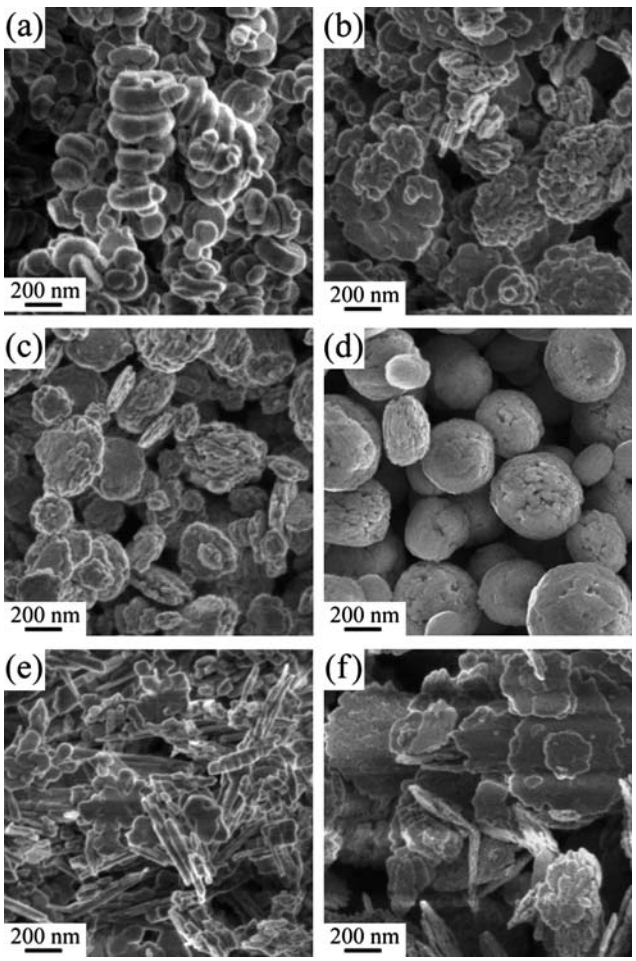

Fig. 5 SEM images of SmF_3 samples, obtained by reaction of Sm^{3+} with NH_4F at 110 °C for 16 h (a) without EDTA; in the presence of (b) 0.5 mmol EDTA, (c) 1 mmol EDTA, (d) 2.5 mmol EDTA, (e) 1.71 mmol 1,6-hexanediamine and (f) 1.71 mmol ammonium citrate.

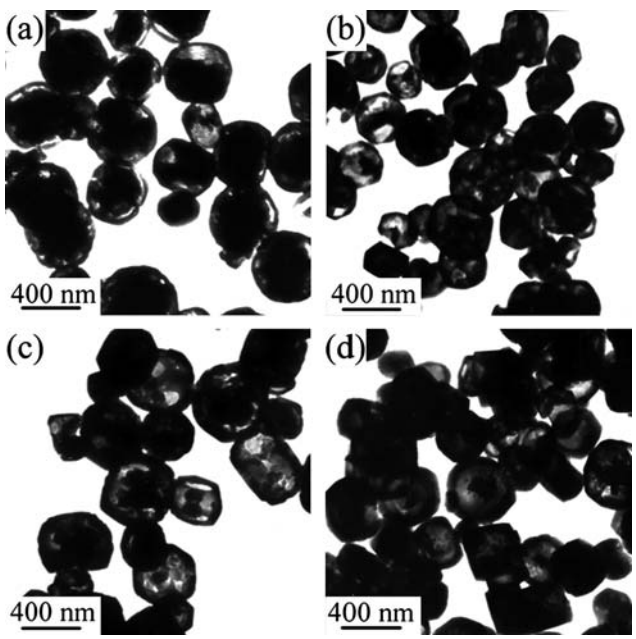

Fig. 6 TEM images of (a) $Sm_{0.75}Eu_{0.25}F_3$, (b) $Sm_{0.5}Eu_{0.5}F_3$, (c) $Sm_{0.25}Eu_{0.75}F_3$ and (d) $Sm_{0.05}Eu_{0.95}F_3$ sub-microcrystals, which were obtained in the solution with molar ratio of Sm^{3+} to Eu^{3+} at 3/1, 1/1, 1/3 and 1/19, respectively.

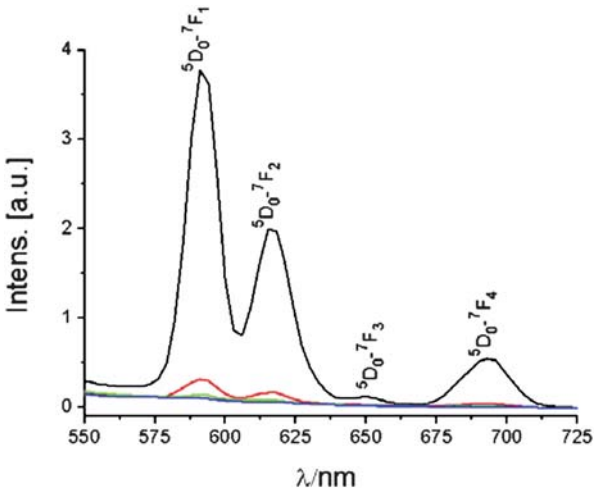

Fig. 7 Emission spectra of Eu-doped SmF_3 rattle-structured sub-microcrystals upon the excitation of 325 nm He–Cd laser. Black line: $Sm_{0.05}Eu_{0.95}F_3$ sub-microcrystals; red line: $Sm_{0.25}Eu_{0.75}F_3$ sub-microcrystals; green line: $Sm_{0.5}Eu_{0.5}F_3$ sub-microcrystals; blue line: $Sm_{0.75}Eu_{0.25}F_3$ sub-microcrystals.

had shown that controlled growth of EuF_3 in similar condition can leads to the formation of hollow hexagonal sub-microdiscs.[29]

In addition, the photoluminescence properties of Eu-doped SmF_3 rattle-structured sub-microcrystals were measured as shown in Fig. 7. It can be seen clearly that the intensity of the emission increases with Eu^{3+} doping level. In the samples doped with high concentration of Eu (black line and red line), the characteristic emissions of Eu^{3+} are observed, which originate from the transitions from the excited $^5D_0$ to the ground states ^7F_j ($j = 1\sim4$). With the decrease of doped-Eu concentration to 0–50%, the luminescence of Eu^{3+} was quenched completely, indicates an efficient energy transfer from Eu^{3+} to Sm^{3+}. In this energy transfer, $^4G_{5/2}$ and $^4F_{3/2}$ states of Sm^{3+} acceptor ions are present to act as acceptors for the excitation energy of the Eu^{3+} ($^5D_1$, $^5D_2$) donor state. Also, such energy transfer behaviour shows that the as-synthesized Eu-doped SmF_3 rattle-structured sub-microcrystals is not a mixture of SmF_3 and EuF_3, but a solid solution, in which Eu^{3+} has successfully incorporated into SmF_3 lattice. Otherwise, the $Eu^{3+} \rightarrow Sm^{3+}$ energy transfer cannot occur in the separated phases.

Conclusions

In summary, SmF_3 rattle-structured sub-micropumpkins have been synthesized in high yield and large-scale *via* a simple complexing-agent-assisted hydrothermal approach. EDTA plays an important role in the formation of SmF_3 rattle-structured sub-micropumpkins. A cooperation of an oriented aggregation process and Ostwald ripening is believed to be the main driving force for the formation of these novel hierarchical architectures. Our study shows that this new type of rattle-structured crystal can be easily doped with other lanthanide ions, which may endow these sub-micropumpkins with novel properties. We believe that this method could be expanded to the synthesis of other rare-earth rattle-structured nano-/microstructues, and thus brings new opportunities to the fast expanding research.

Experimental

All the chemicals and reagents were analytical grade, purchased from Sinopharm Chemical Reagent Co., Ltd. (Shanghai, China), and used without further purification. Deionized water was used throughout. In a typical synthesis, EDTA solution was obtained by dissolving 500 mg EDTA in 6.5 mL of 1 M ammonium hydroxide solution. NH_4F solution was obtained by dissolving 200 mg NH_4F in 7 mL water–ethanol (2/5, v/v). Sm_2O_3 (0.5 mmol) was completely dissolved in 6.8 mL of 0.74 M HNO_3 to form $Sm(NO)_3$ solution. Then, the EDTA solution and 10 mL ethanol were added to the obtained $Sm(NO)_3$ solution in sequence to get Sm-EDTA solution. After 5 min ultrasonic bath, the NH_4F solution was introduced into the Sm-EDTA solution. Subsequently, the mixed system was sonolyzed for 5 min to ensure homogeneous dispersion of all reagents in the solutions and transferred into a Teflon-lined autoclave. After the autoclave was tightly sealed and heated at 110 °C for 16 h, the system was allowed to cool to room temperature naturally. The as-obtained white precipitate was collected, washed with distilled water and absolute ethanol several times, and finally dried at 110 °C in air for 0.5 h. About 197.5 mg SmF_3 rattle-structured sub-micropumpkins could be obtained. Using the same procedures, the concentration of EDTA, time scale, and the composition of metal precursors were varied in the experiments to obtain products with a desired morphology and composition.

XRD patterns of the products were recorded on a Shimadzu XRD-6000 X-ray diffractometer with CuKα radiation (λ = 0.15406 nm) at a scanning rate of 0.1° s^{-1} in the 2θ range from 20–80°. TEM images were obtained on a JEM-200CX transmission electron microscope, with an accelerating voltage of 200 kV. SEM images were acquired from a Hitachi S-4800 scanning electron microscope. HRTEM image and EDX analysis was taken on a JEM 2010 high-resolution transmission electron microscope with an energy-dispersive X-ray spectroscope. Luminescent spectra were carried out on an SLM48000DSCF photoluminescence spectrometer and an excitation wavelength of 325 nm using a He–Cd laser.

Acknowledgements

This work is supported by the National Natural Science Foundation of P. R. China. (20535020, 20671051, 20721002 and 90813020) and the National Basic Research Program of P. R. of China (2007CB925102).

References

1 Y. N. Xia, P. D. Yang, Y. G. Sun, Y. Y. Wu, B. Mayers, B. Gates, Y. D. Yin, F. Kim and H. Q. Yan, *Adv. Mater.*, 2003, **15**, 353–389.
2 L. J. Lauhon, M. S. Gudiksen, D. L. Wang and C. M. Lieber, *Nature*, 2002, **420**, 57–61.
3 K. A. Dick, K. Deppert, M. W. Larsson, T. Martensson, W. Seifert, L. R. Wallenberg and L. Samuelson, *Nat. Mater.*, 2004, **3**, 380–384.
4 X. Y. Kong, Y. Ding, R. Yang and Z. L. Wang, *Science*, 2004, **303**, 1348–1351.
5 X. W. Lou, Y. Wang, C. L. Yuan, J. Y. Lee and L. A. Archer, *Adv. Mater.*, 2006, **18**, 2325–2329.
6 W. M. Zhang, J. S. Hu, Y. G. Guo, S. F. Zheng, L. S. Zhong, W. G. Song and L. J. Wan, *Adv. Mater.*, 2008, **20**, 1160–1165.
7 X. W. Lou and L. A. Archer, *Adv. Mater.*, 2008, **20**, 1853–1858.
8 O. Kreft, A. G. Skirtach, G. B. Sukhorukov and H. Möhwald, *Adv. Mater.*, 2007, **19**, 3142–3145.

9 O. Kreft, M. Prevot, H. Möhwald and G. B. Sukhorukov, *Angew. Chem., Int. Ed.*, 2007, **46**, 5605–5608.
10 W. R. Zhao, H. R. Chen, Y. S. Li, L. Li, M. D. Lang and J. L. Shi, *Adv. Funct. Mater.*, 2008, **18**, 2780–2788.
11 J. H. Gao, G. L. Liang, J. S. Cheung, Y. Pan, Y. Kuang, F. Zhao, B. Zhang, X. X. Zhang, E. X. Wu and B. Xu, *J. Am. Chem. Soc.*, 2008, **130**, 11828–11833.
12 S. Ikeda, S. Ishino, T. Harada, N. Okamoto, T. Sakata, H. Mori, S. Kuwabata, T. Torimoto and M. Matsumura, *Angew. Chem., Int. Ed.*, 2006, **45**, 7063–7066.
13 F. Iskandar, A. B. D. Nandiyanto, K. M. Yun, C. J. Hogan, K. Okuyama and P. Biswas, *Adv. Mater.*, 2007, **19**, 1408–1412.
14 H. G. Zhang, Q. S. Zhu, Y. Zhang, Y. Wang, L. Zhao and B. Yu, *Adv. Funct. Mater.*, 2007, **17**, 2766–2771.
15 Y. Zhao and L. Jiang, *Adv. Mater.*, 2009, **21**, 3621–3638.
16 B. Liu and H. C. Zeng, *Small*, 2005, **1**, 566–571.
17 B. P. Jia and L. Gao, *J. Phys. Chem. C*, 2008, **112**, 666–671.
18 B. P. Jia and L. Gao, *J. Cryst. Growth*, 2007, **303**, 616–621.
19 R. Qiao, X. L. Zhang, R. Qiu, J. C. Kim and Y. S. Kang, *Chem.–Eur. J.*, 2009, **15**, 1886–1892.
20 Y. H. Zheng, Y. Cheng, Y. S. Wang, L. H. Zhou, F. Bao and C. Jia, *J. Phys. Chem. B*, 2006, **110**, 8284–8288.
21 X. X. Yu, J. G. Yu, B. Cheng and B. B. Huang, *Chem.–Eur. J.*, 2009, **15**, 6731–6739.
22 Y. B. Chen, L. Chen and L. M. Wu, *Cryst. Growth Des.*, 2008, **8**, 2736–2740.
23 X. L. Tian, J. Li, K. Chen, J. Han and S. L. Pan, *Cryst. Growth Des.*, 2009, **9**, 4927–4932.
24 W. S. Wang, L. Zhen, C. Y. Xu and W. Z. Shao, *Cryst. Growth Des.*, 2009, **9**, 1558–1568.
25 W. S. Wang, L. Zhen, C. Y. Xu, B. Y. Zhang and W. Z. Shao, *J. Phys. Chem. B*, 2006, **110**, 23154–23158.
26 X. Wang, J. Zhuang, Q. Peng and Y. D. Li, *Inorg. Chem.*, 2006, **45**, 6661–6665.
27 S. Heer, O. Lehmann, M. Haase and H. U. Gudel, *Angew. Chem., Int. Ed.*, 2003, **42**, 3179–3182.
28 J. W. Stouwdam and F. C. J. M. van Veggel, *Nano Lett.*, 2002, **2**, 733–737.
29 Z. M. Chen, Z. R. Geng, D. L. Shao, Y. H. Mei and Z. L. Wang, *Anal. Chem.*, 2009, **81**, 7625–7631.
30 K. B. Zhou, X. Wang, X. M. Sun, Q. Peng and Y. D. Li, *J. Catal.*, 2005, **229**, 206–212.
31 G. S. Yi, H. C. Lu, S. Y. Zhao, Y. Ge, W. J. Yang, D. P. Chen and L. H. Guo, *Nano Lett.*, 2004, **4**, 2191–2196.
32 H. C. Lu, G. S. Yi, S. Y. Zhao, D. P. Chen, L. H. Guo and J. Cheng, *J. Mater. Chem.*, 2004, **14**, 1336–1341.
33 S. Sivakumar, P. R. Diamente and F. C. J. M. van Veggel, *Chem.–Eur. J.*, 2006, **12**, 5878–5884.
34 L. Y. Wang, R. X. Yan, Z. Y. Huo, L. Wang, J. H. Zeng, J. Bao, X. Wang, Q. Peng and Y. D. Li, *Angew. Chem., Int. Ed.*, 2005, **44**, 6054–6057.
35 R. X. Yan and Y. D. Li, *Adv. Funct. Mater.*, 2005, **15**, 763–770.
36 G. Y. Li, Y. H. Ni, J. M. Hong and K. M. Liao, *CrystEngComm*, 2008, **10**, 1681–1686.
37 M. Wang, Q. L. Huang, J. M. Hong, X. T. Chen and Z. L. Xue, *Cryst. Growth Des.*, 2006, **6**, 2169–2173.
38 M. M. Lezhnina, T. Jüstel, H. Kätker, D. U. Wiechert and U. H. Kynast, *Adv. Funct. Mater.*, 2006, **16**, 935–942.
39 X. Wang and Y. D. Li, *Angew. Chem., Int. Ed.*, 2003, **42**, 3497–3500.
40 X. Wang and Y. D. Li, *Chem.–Eur. J.*, 2003, **9**, 5627–5635.
41 J. L. Lemyre and A. M. Ritcey, *Chem. Mater.*, 2005, **17**, 3040–3043.
42 Y. W. Zhang, X. Sun, R. Si, L. P. You and C. H. Yan, *J. Am. Chem. Soc.*, 2005, **127**, 3260–3261.
43 L. Zhu, X. M. Liu, J. Meng and X. Q. Cao, *Cryst. Growth Des.*, 2007, **7**, 2505–2511.
44 Z. M. Chen, Z. R. Geng, M. L. Shi, Z. H. Liu and Z. L. Wang, *CrystEngComm*, 2009, **11**, 1591–1596.
45 C. X. Li, J. Yang, P. P. Yang, H. Z. Lian and J. Lin, *Chem. Mater.*, 2008, **20**, 4317–4326.
46 A. Kar, A. Datta and A. Patra, *J. Mater. Chem.*, 2010, **20**, 916–922.
47 D. B. Yu, X. Q. Sun, J. W. Zou, Z. R. Wang, F. Wang and K. Tang, *J. Phys. Chem. B*, 2006, **110**, 21667–21671.
48 B. P. Jia and L. Gao, *Cryst. Growth Des.*, 2008, **8**, 1372–1376.
49 C. H. Huang, *Coordination Chemistry of Rare Earth Elements*, Science Publishing Press: Beijing, 1997, ch. 2, pp. 29; ch. 5, pp. 223.
50 J. H. Zeng, Z. H. Li, J. Su, L. Y. Wang, R. X. Yan and Y. D. Li, *Nanotechnology*, 2006, **17**, 3549–3555.